Article

Fabrication of Robust Waterborne Superamphiphobic Coatings with Antifouling, Heat Insulation, and Anticorrosion

Zeting Qiao, Guoyu Ren,* Xiaodong Chen, Yanli Gao, Yun Tuo, and Cuiying Lu

Read Online

ACCESS | Metrics & More | Article Recommendations | Supporting Information

● Low thermal conductivity filler ⌇⌇ Organic molecular chain ⟋⟍ PTFE ⋀ Silicate ⋁ Curing agent
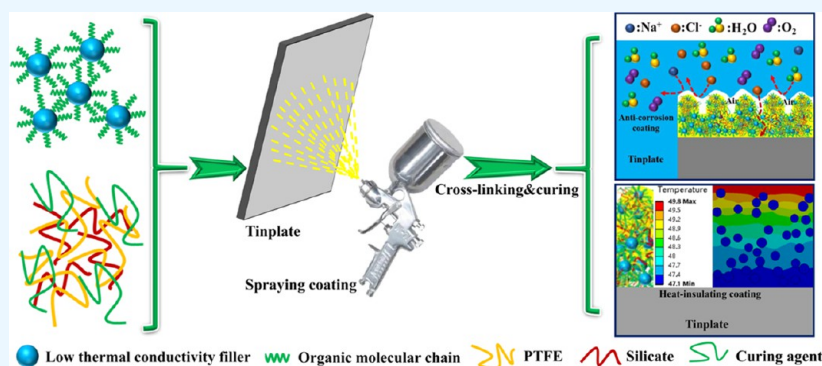
ABSTRACT: Water-based superamphiphobic coatings that are environmentally friendly have attracted tremendous attention recently, but their performances are severely limited by dispersibility and mechanical durability. Herein, a dispersion of poly(tetrafluoroethylene)/SiO$_2$@cetyltrimethoxysilane&sodium silicate-modified aluminum tripolyphosphate (PTFE/SiO$_2$@ CTMS&Na$_2$SiO$_3$-ATP) superamphiphobic coatings was formed by mechanical dispersion of poly(tetrafluoroethylene) emulsion (PTFE), modified silica emulsion (SiO$_2$@CTMS), sodium silicate (Na$_2$SiO$_3$), and modified aluminum tripolyphosphate (modified ATP). The four kinds of emulsions were mixed together to effectively solve the dispersity of waterborne superamphiphobic coatings. Robust waterborne superamphiphobic coatings were successfully obtained by one-step spraying and curing at 310 °C for 15 min, showing strong adhesive ability (grade 1 according to the GB/T9286), high hardness (6H), superior antifouling performance, excellent impact resistance, high-temperature resistance (<415 °C), anticorrosion (immersion of strong acid and alkali for 120 h), and heat insulation. Remarkably, the prepared coating surface showed superior wear resistance, which can undergo more than 140 abrasion cycles. Moreover, the composite coating with 35.53 wt % SiO$_2$@CTMS possesses superamphiphobic properties, with contact angles of 160 and 156° toward water and glycerol, respectively. The preparation method of superamphiphobic coatings may be expected to present a strategy for the preparation of multifunctional waterborne superamphiphobic coatings with excellent properties and a simple method.

1. INTRODUCTION

Due to excellent repellency performance for water and oil,[1−4] superamphiphobic coatings have wide application prospects in self-cleaning,[5−9] drag reduction,[10,11] anti-graffiti,[12−14] anti-corrosion,[15−18] anti-icing,[19−21] petroleum pipeline,[22] etc. Superamphiphobic surfaces with extremely excellent properties need to possess low surface energy and a hierarchical roughness structure.[23,24] Water-based superamphiphobic coatings are environmentally friendly and have attracted many researchers' attention.[25,26] Nevertheless, the dispersion of hydrophobic substances in water is poor, which is not conducive to the performance of the coatings.[27] Therefore, improving the dispersibility is an important and critical factor for water-based superamphiphobic coatings to replace solvent-borne superamphiphobic coatings.[28]

So far, many researchers have tried to solve the problem of dispersion. Avijit et al. mixed water-dispersed clay sheets (6 wt

%) with two different functional silanes (1H,1H,2H,2H-perfluorooctyltriethoxysilane and 3-(2-aminoethylamino) pro-pyltrimethoxysilane) and kept under vigorous stirring con-ditions for 6 h to obtain the coating dispersion.[29] Lozhechnikova et al. synthesized anionic wax particles in combination with cationic ZnO nanoparticles by adjusting pH to fabricate superhydrophobic coatings.[30] Furthermore, some works reported simple methods to develop aqueous dispersion. Silica nanoparticles were dispersed in an O/W emulsion and
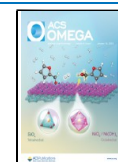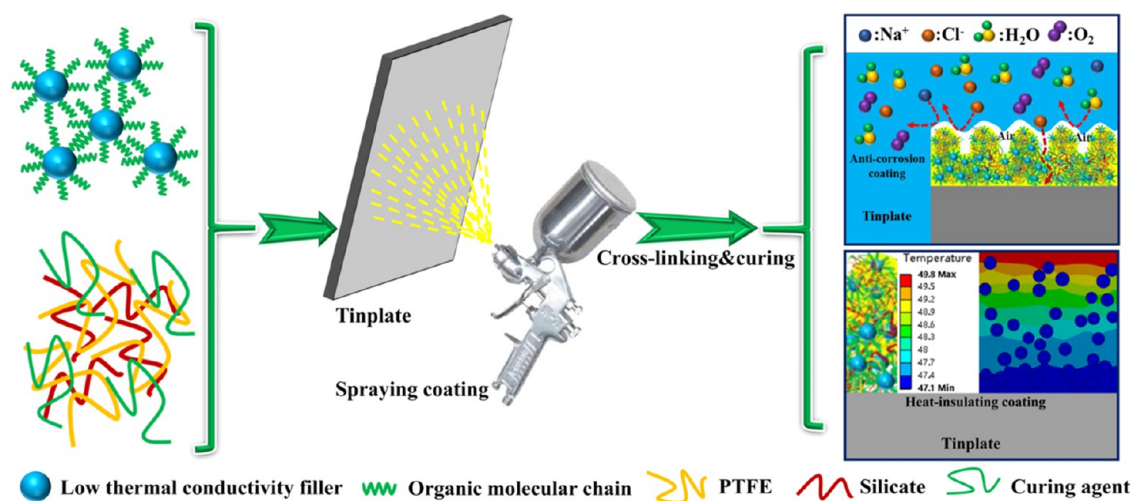
Figure 1. Strategy of waterborne superamphiphobic coatings enhances the hardness and wear resistance of the coatings and takes into account the impact resistance, high-temperature resistance, anticorrosion, and heat insulation.

coated on different substrates to prepare aqueous superhydrophobic surfaces.[31−33] However, there are few reports on the durability of superhydrophobic surfaces. Moreover, the dispersion of superamphiphobic coatings is rarely discussed.

The mechanical strength of a coating is extremely important, which determines the durability of the coating with a hierarchical roughness structure.[34] Li et al. sprayed polyurethane and SiO$_2$@HD-POS (hexadecylpolysiloxane-modified SiO$_2$) aqueous solution on a glass slide to prepare a superhydrophobic surface. This coating owned self-repairing ability and wear resistance, but the hardness of the coating was not mentioned.[35] Zhao et al. fabricated a superhydrophobic coating with 6H by a silicone acrylate copolymer emulsion, and silica nanoparticles were modified with 1H,1H,2H,2H-perfluorododecyltriethoxysilane in the emulsion to air dry. But wear resistance has not been explored.[36] In addition, some works are attempted to solve the durability of a coating with a hierarchical roughness structure, but the methods are complex and damage the mechanical properties of the substrate.[37−39] Therefore, it is particularly important to provide a simple method to prepare superamphiphobic surfaces and consider the overall properties of the coatings.

In this paper, the dispersion of nanosilica was modified by cetyltrimethoxysilane (CTMS) to reduce coating surface energy and enhance adhesion. To solve the dispersion and the durability of water-based coatings, the water-based dispersion was formed by the mechanical dispersion of the PTFE emulsion, modified silica (SiO$_2$@CTMS), sodium silicate, and modified ATP. The four kinds of emulsions were mixed together to effectively solve the dispersity of waterborne superamphiphobic coatings. Robust superamphiphobic surfaces with micro/nanohierarchical structures were successfully fabricated by a simple one-step spraying method and curing at 310 °C for 15 min. Due to nanosilica lubrication and film hardness, the PTFE/SiO$_2$@CTMS&Na$_2$SiO$_3$-ATP composite coating showed excellent wear resistance, which can undergo 140 cycles of wear and still show high contact angles (CAs) and sliding angles (SAs) for water (CAs = 152 ± 0.8°, SAs = 11 ± 0.9°) and glycerol (CAs = 149 ± 0.7°, SAs = 22 ± 0.6°). Because of the refractories of modified silica, sodium silicate, and modified ATP,[40−43] the PTFE/SiO$_2$@CTMS&Na$_2$SiO$_3$-ATP composite coating has the character-

istics of high-temperature resistance (within 415 °C) and insulation. Furthermore, it showed strong adhesive ability (grade 1), high hardness (6H), superior antifouling performance (100 cycles of slurry and glycerol), excellent impact resistance, heat insulation, and anticorrosion (immersion of strong acid and alkali for 120 h). This work is expected to provide a preparation strategy for multifunctional waterborne superamphiphobic coatings with excellent properties and a simple method (Figure 1). It not only enhances the hardness and wear resistance of the coatings but also takes into account impact resistance, high-temperature resistance, heat insulation, and anticorrosion.

2. EXPERIMENTAL SECTION

2.1. Materials. Hydrochloric acid and potassium hydroxide were purchased from Tianjin Kemiou Chemical Reagent Co., Ltd. (China). The PTFE emulsion (60 wt %, TE3893) was provided by DuPont. Tetraethyl orthosilicate was provided by Tianjin Damao Chemical Reagent Factory (China). Ammonia and anhydrous ethanol were purchased from Tianjin Tianli Chemical Reagent Co., Ltd. (China). Modified aluminum tripolyphosphate (P$_2$O$_5$: 48−52 wt %, Al$_2$O$_3$: 11−14 wt %, ZnO: 18−22 wt %) was supplied by Shandong Yousuo Chemical Technology Co., Ltd. (China). Cetyltrimethoxysilane (CTMS) was supplied by Nanjing Youpu Chemical Co., Ltd. (China). Sodium chloride, glycerol, and sodium silicate were purchased from Tianjin Zhiyuan Chemical Reagent Co., Ltd. (China).

2.2. Preparation of Modified Silica Nanoparticles. Water (150 g), absolute ethanol (60 g), and tetraethyl orthosilicate (30 g) were dispersed in a 500 mL beaker. The above mixed solution was placed in a water bath (magnetic stirring) and heated to 40 °C. Ammonia water (35 g, 1 drop per second) was dropped at 40 °C for 2 h. Subsequently, cetyltrimethoxysilane (CTMS, 10 g) was added to the above solution at 40 °C for 2.5 h. After completion, the dispersion of modified silica (90 wt %) was obtained by centrifuging with a high-speed centrifuge (four times) to remove residual anhydrous ethanol and ammonia.

The prepared dispersion of modified silica was milky white (Figure S1a). The dispersion of modified silica could be stored
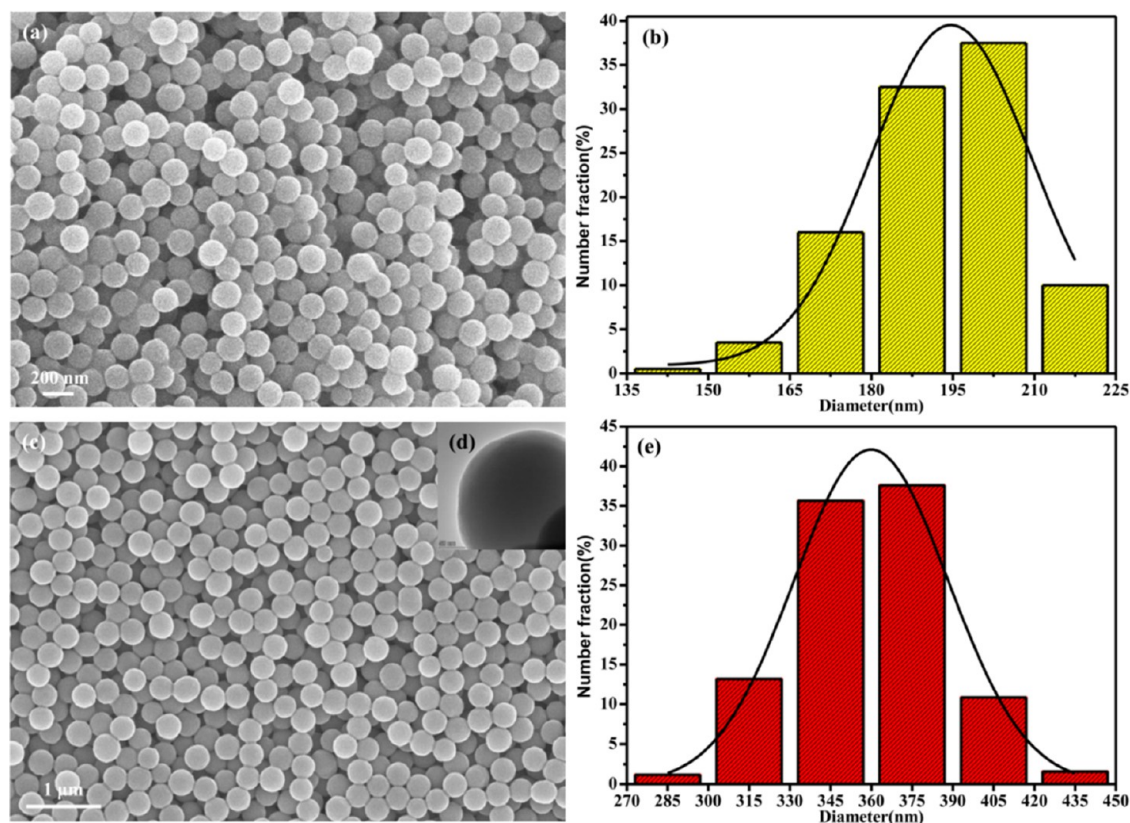
Figure 2. Modified silica with different particle sizes: (a, b) 192 nm modified silica and (c−e) 360 nm modified silica.

for 180 days (Figure S1b). It was clear that the dispersion was not layered for a long time.

2.3. Preparation of the Composite Coating. The choice of the mass ratio of the four substances was critical for the experiment. First, the weights of the PTFE emulsion and modified silica dispersion were definite: under the condition of 50 g of PTFE (60 wt %) and 35 g of modified silica dispersion (90 wt %). Second, the ratio and dosage of sodium silicate and modified ATP (20 wt %) were determined by many tests. The amounts of sodium silicate and modified ATP were determined when the composite coating was not cracked and the spray was not blocked, and the hardness reached 6H. The reaction was extremely fast between sodium silicate and modified ATP. So the weight of modified ATP was lower. The mass ratio of sodium silicate and modified ATP was 1:4. The weights of sodium silicate and modified ATP (20 wt %) were 15 and 20 g, respectively. Finally, by changing the weight of the modified silica emulsion (90 wt %), the upper limit of the amount of modified silica emulsion was determined when the composite coating was cracked.

The surface of tinplate was polished with 200 mesh sandpaper to remove oil and rust. The residue was blown away with a blower for standby. The PTFE emulsion (50 g, 60 wt%), modified silica emulsion (30 g, 90 wt %), modified ATP (20 g, 20 wt %), and sodium silicate (15 g) were added together and stirred for 10 min to disperse. Nano/micro-hierarchical surface structures were obtained by spraying the coating dispersion on tinplate and curing at 310 °C for 15 min.

Each component of the PTFE/SiO$_2$@CTMS&ATP dispersion was evenly dispersed in the aqueous solution (Figure S2a). After 90 min, the coating dispersion was found to be stratified (Figure S2b). Even if the coating dispersion was

layered, it can be returned to its original state by a high-speed stirrer to maintain good dispersion (Figure S2c). Therefore, according to the results, modified silica dispersion and PTFE/SiO$_2$@CTMS&ATP dispersion both have long-term storage.

2.4. Characterization. The CAs and SAs of the coating were measured by the pendant drop method with approximately 5 μL of water and glycerol. A contact angle meter (JC2000C1, Shanghai Zhongchen Digital Technology Equipment Co., Ltd.) was accepted for measuring five places of each sample. The reported values were the average measurements from five different locations. The morphology of modified nanosilica was observed by a field emission scanning transmission electron microscope (TEM, JEM-2100f) and a field emission scanning electron microscope (SEM, sigma 300). Nano Measurer software was used to do the size distribution. Furthermore, Fourier transform infrared spectroscopy (FT-IR, Bruker Tensor 27) was used to judge the grafting of cetyltrimethoxysilane onto nanosilica, and thermogravimetry (LABSYS EVO) was adopted to measure the grafting rate of nanosilica. The thermal conductivity and heat flow density of nanosilica were obtained by a thermal conductivity measuring instrument (Hot Disk TPS2500S).

The morphology of the PTFE/SiO$_2$@CTMS&Na$_2$SiO$_3$-ATP composite coating was observed by a field emission scanning electron microscope (SEM, sigma 300). 3D surface morphology images and thickness of the composite coating were obtained by a 3D profiler (KLA-Tencore, D-120). The test of antifouling performance was to immerse and lift (100 cycles) the sample in glycerol and slurry (40 wt %). It observed the degree of cleanliness for the surface of the composite coating. Moreover, the stability of the coating was tested by severe glycerol immersion (10 days). The coefficient of heat
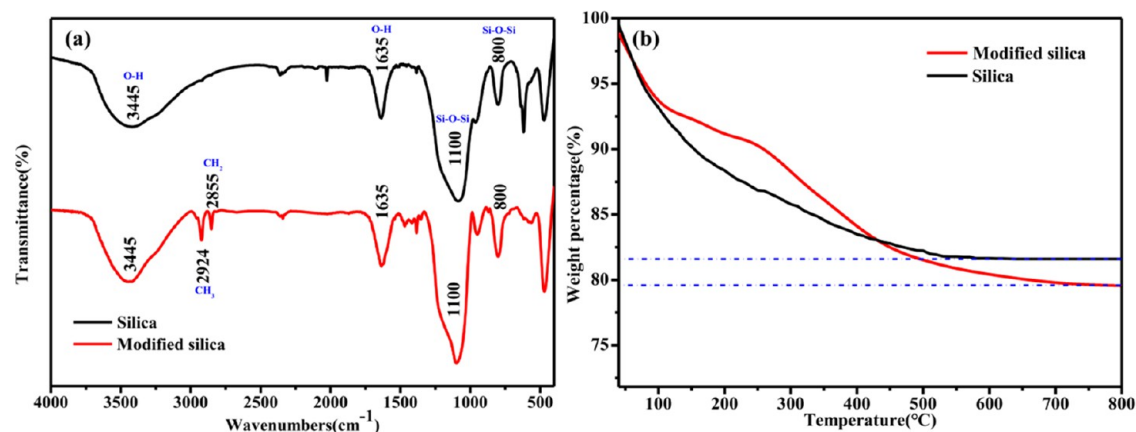
Figure 3. Characterization of modified silica nanoparticles: (a) FT-IR spectra and (b) thermogravimetry of modified silica nanoparticles.
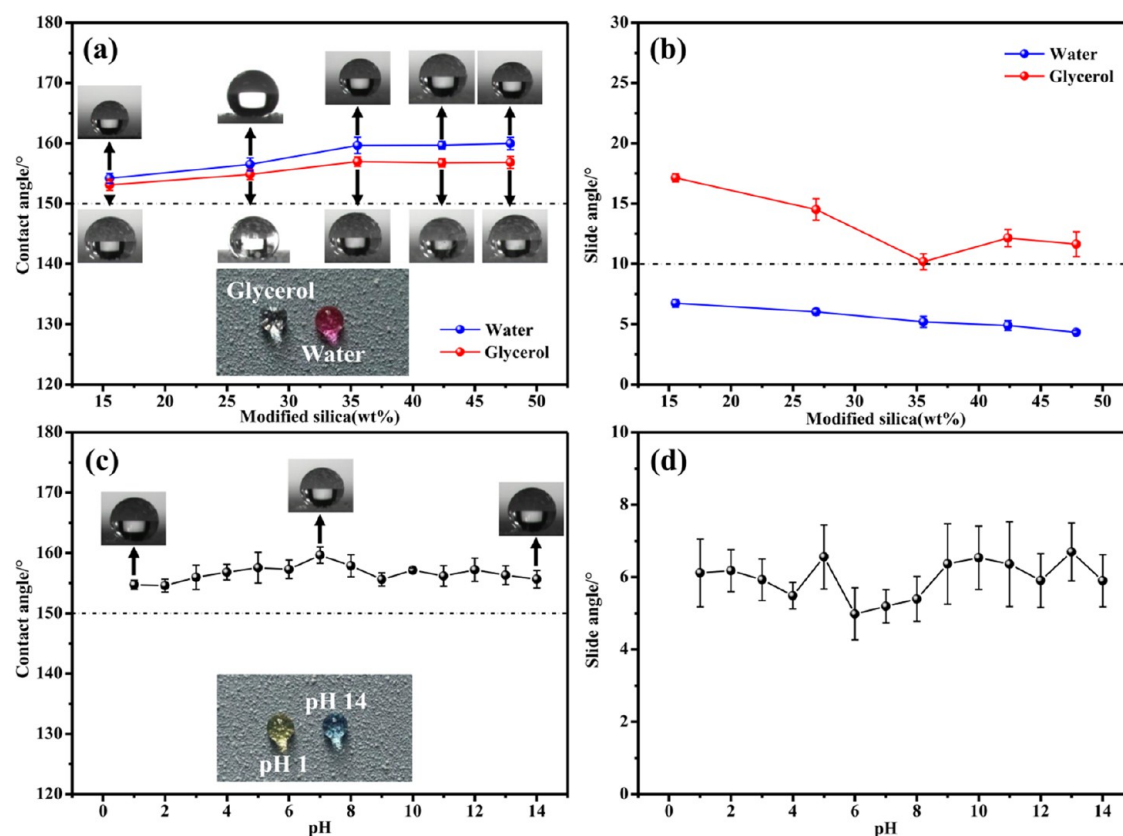
Figure 4. Wettability of composite coating. (a, b) CAs and SAs of the composite coating with different contents of modified silica nanoparticles to water and glycerol. (c, d) CAs and SAs of the PTFE/SiO$_2$@CTMS&Na$_2$SiO$_3$-ATP composite coating to different pH solutions.

conductivity was calculated according to the principle of multilayer flat wall and thermal resistance in series methods (DM-3615 thermal conductivity tester by pulse width modulation, Shanghai Dongmao Electronic Technology Co., Ltd.). Temperature distribution and heat flux were calculated by the finite element method.

According to GB/T6739, the PTFE/SiO$_2$@CTMS&Na$_2$SiO$_3$-ATP composite coating was tested by a pencil hardness tester to evaluate film hardness (QHQ type, Dongguan Huaguo Precision Instrument Co., Ltd.). The cross-cut tape test of the composite coating was conducted to evaluate the adhesion according to GB/T9286. According to GB/T1732, the impact resistance of the composite coating was

tested by a paint film impact instrument (QCJ-50/100, Tianjin World Expo Weiye Chemical Glass Instrument Co., Ltd.).

The composite coating was soaked in hydrochloric acid (pH 1) and potassium hydroxide (pH 14) for 24, 48, 72, 96, and 120 h, separately. The trend of CAs and SAs for hydrochloric acid (pH 1) and potassium hydroxide (pH 14) were measured (after the test, all samples were dried for wettability evaluation under the same conditions). To further evaluate the corrosion resistance of the coating, the potentiodynamic polarization curve and electrochemical impedance spectroscopy (EIS) were performed on an electrochemical workstation (CHI760E type, Shanghai Chenhua Instrument Co., Ltd., the initial potential was −1 V, the final potential was 0 V, and the scanning rate was 0.01 V/s).
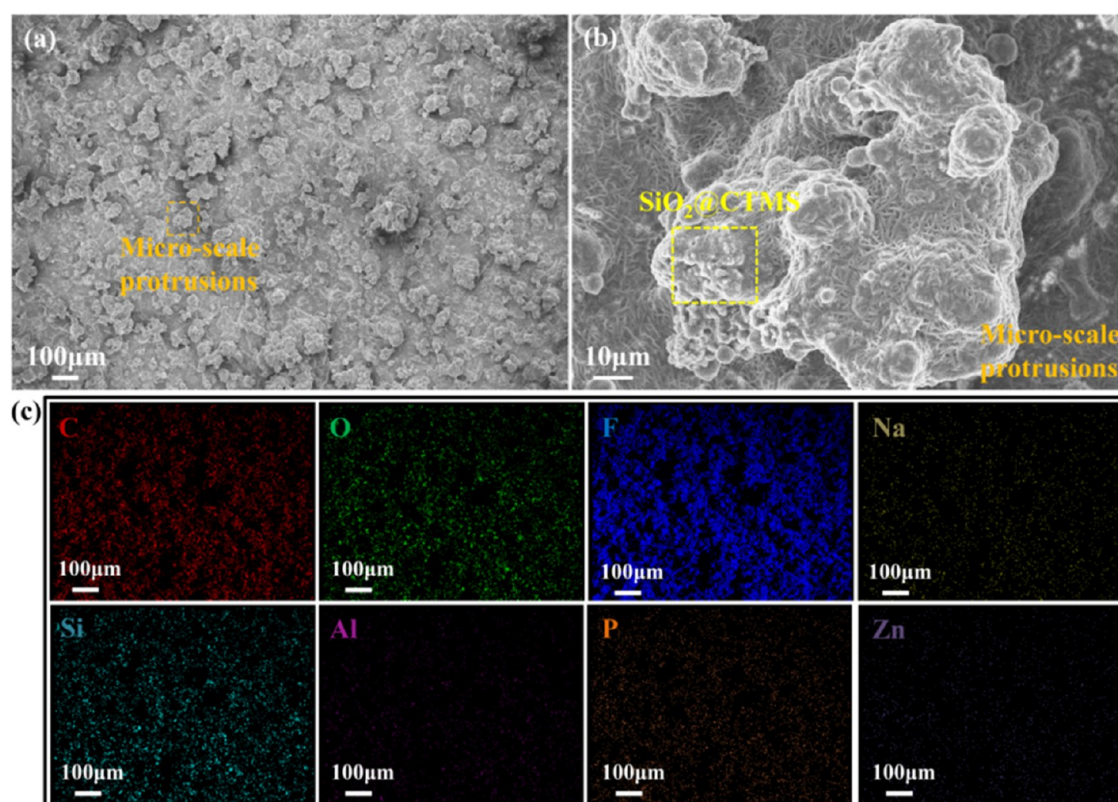
Figure 5. SEM of the PTFE/SiO$_2$@CTMS&Na$_2$SiO$_3$-ATP composite coating. (a, b) SEM of the PTFE/SiO$_2$@CTMS&Na$_2$SiO$_3$-ATP composite coating and the emulsion protrusion. (c) Element distribution of the PTFE/SiO$_2$@CTMS&Na$_2$SiO$_3$-ATP composite coating.

3. RESULTS AND DISCUSSION

3.1. Characterization of Modified Silica. Two kinds of modified silica particles (the average particle size was 192 nm, and the average particle size was 360 nm) were synthesized. From the observation of the morphology of the two particle sizes, it was found that the modified silica with an average particle size of 192 nm was easier to agglomerate than the modified silica with an average particle size of 360 nm (Figure 2). The composite coating was prepared by 192 nm modified silica dispersion and 360 nm modified silica dispersion separately. The CAs (glycerol, water) of the two kinds of particle sizes did not change significantly, but 360 nm modified silica showed relatively high CAs (Figure S3). Therefore, the 360 nm particle size was used for the later experiment.

The surface of the modified silica particles was relatively smooth (Figure 2c). Cetyltrimethoxysilane was uniformly coated on the surface of SiO$_2$ particles, which showed almost no agglomerated structure. The synthesized silica particle had an obvious core−shell structure, and the shell thickness was about 20 nm (Figure 2d). The particle size was mainly distributed between 345 and 375 nm (average particle size, 360 nm), showing that the size distribution of modified silica was uniform (Figure 2e). Compared with the FT-IR spectra of silica (Figure 3a), the FT-IR spectra of modified silica indicated that different absorption peaks were located at 2855 cm^{-1} (symmetric tensile vibration peak) and 2924 cm^{-1} (antisymmetric tensile vibration peak), which belonged to methylene (CH$_2$) and methyl (CH$_3$), respectively.[44,45] The results testified that cetyltrimethoxysilane had successfully modified silica. The mass percentage of silica-branched cetyltrimethoxysilane was measured by thermogravimetry.

Compared with unmodified silica, the additional weight loss rate of modified silica was about 2.01% (Figure 3b).

3.2. Wettability Analysis of the Coating. The waterborne superamphiphobic coatings were prepared by spraying the suspension of the filler/polymer with different proportions on the surface of tinplate and curing at 310 °C for 15 min. Modified silica increased the roughness of the coating and reduced the surface energy. Therefore, modified silica was added to PTFE&Na$_2$SiO$_3$-ATP with different loadings varying from 15.52 to 47.87 wt %. The water CAs were transformed from 154 ± 0.8 to 160 ± 0.7° and the glycerol CAs from 153 ± 0.5 to 156 ± 0.9° as the modified silica filler increased from 15.52 to 47.87 wt % (Figure 4a). The SAs of both water and glycerol droplets reduced gradually with increasing modified silica (Figure 4b). Because the composite coating has a heterogeneous rough surface (Figure 13a) and low surface energy, making the composite coating exhibit high CAs and low SAs. It conforms to the Cassie−Baxter model.[46] The droplets do not infiltrate the rough structure and form a stable solid−liquid-vapor interface. The composite coating shows excellent moisture resistance. A low solid−liquid contact area fraction indicates high CAs and excellent hydrophobicity. This is basically consistent with the results of the apparent contact angle (Figure 4a). When the content of modified silica in the coating system reaches 52.43 wt %, the cross-linking curing of sodium silicate and modified ATP is prevented to reduce the bonding strength of the coating, resulting in the cracking of the coating (Figure S4). Generally considering, the coating has optimized superamphiphobicity when the modified silica filler is 35.53 wt %. It will be taken as the further research object in the
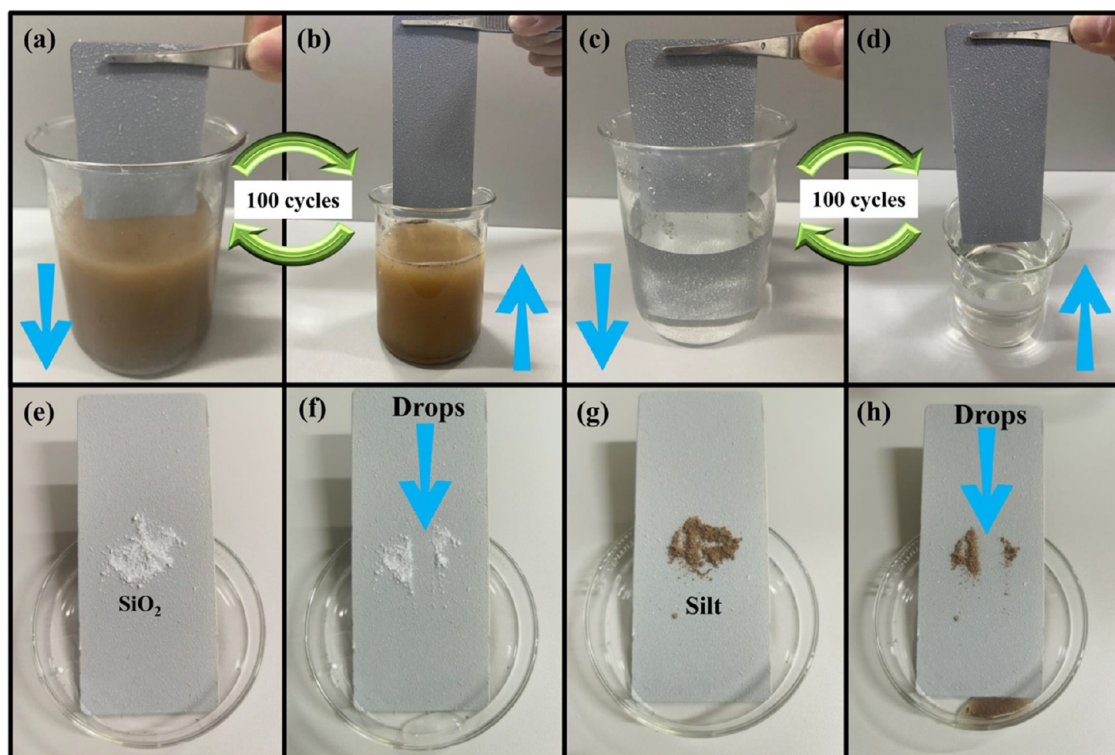
Figure 6. Self-cleaning and antipollution test. (a, b) Slurry (40 wt %) antipollution test. (c, d) Glycerol antipollution test. (e, f) Self-cleaning test of 100 nm silica. (g, h) Self-cleaning test of silt.

following and abbreviated as the PTFE/SiO$_2$@CTMS&Na$_2$SiO$_3$-ATP composite coating.

The repellency of corrosive droplets was tested, so as to comprehensively evaluate the scope of application of the PTFE/SiO$_2$@CTMS&Na$_2$SiO$_3$-ATP composite coating. High CAs and low SAs for the droplets in the range of pH 1−14 are shown in Figure 4c,d. The composite coating surface maintains superamphiphobicity for corrosive droplets. According to the results, it can be concluded that the prepared organic/inorganic hybrid superamphiphobic coatings have excellent liquid repellency.

3.3. Analysis of Morphology and Element. The excellent performance of superamphiphobic coatings needs to meet the requirements of the hierarchical roughness structure and extremely low surface energy. Sodium silicate and the curing agent (modified ATP) were added to the coating system, and the viscosity of coating dispersion was increased, which was easier to form aggregates to form a rough structure in the process of spraying. After high-temperature curing, a thickness of the composite coating of 40 μm was obtained (Figure S5a,c), and the composite coating surface had emulsion protrusions similar to the natural lotus leaf (Figure 5a). The surface of the emulsion protrusion was embedded with modified silica, and the rough morphology was similar to rice particles, which jointly formed nano/microhierarchical structures that intercepted air to form a stable gas film (Figure 5b).[47−50] It was beneficial to fabricate the optimized superamphiphobic surfaces. As displayed in Figure 5c, elements were distributed on the surface of the PTFE/SiO$_2$@CTMS&Na$_2$SiO$_3$-ATP composite coating. The coating contained eight elements, among which fluorine was a low-surface-energy element provided by PTFE. The composition

analysis of the composite coating is displayed in Figures S6−S8 and Table S1.

3.4. Analysis of Antifouling Performance. The most attractive feature of superamphiphobic coatings is the remarkable pollution resistance. As shown in Figure 6a,b, the PTFE/SiO$_2$@CTMS&Na$_2$SiO$_3$-ATP composite coating was repeatedly soaked in a slurry (40 wt %) 100 times, and no sediment particles remained on the coating surface (slurry dumping: Movie S1). Similarly, the coating was repeatedly immersed in glycerol 100 times (Figure 6c,d), but the coating surface was intact, and no glycerol remained (Movie S2, glycerol dumping: Movie S3). Furthermore, silica (50 nm) and sediment were placed in the middle of the composite coating with an inclination of 30°, and a rubber dropper dropped deionized water from the top of the sample plate. It was clearly observed that pollutants were taken away quickly in the process of droplet falling (Figure 6e−h). The pollutant removal method of the sample plate is the same as that of a lotus leaf, which proves that the surface of the PTFE/SiO$_2$@CTMS&Na$_2$SiO$_3$-ATP composite coating successfully imitates the surface of a lotus leaf. Considering that the gas film on the surface of the PTFE/SiO$_2$@CTMS&Na$_2$SiO$_3$-ATP composite coating will be renewed again during each coating dipping and pulling process, which will affect the judgment of antifouling performance. Therefore, a more rigorous glycerol immersion test was carried out to evaluate the antifouling performance of the coating. The composite coating was soaked in glycerol for different times (2 days, 4 days, 6 days, 8 days, and 10 days) to measure the CAs and SAs (water, glycerol). It was worth mentioning that the PTFE/SiO$_2$@CTMS&Na$_2$SiO$_3$-ATP composite coating still had excellent repellency to glycerol (CAs = 151 ± 0.9°, SAs = 15 ± 1°) and water (CAs = 154 ± 2.7°, SAs = 9 ± 0.5°) after 10 days (Figure 7).
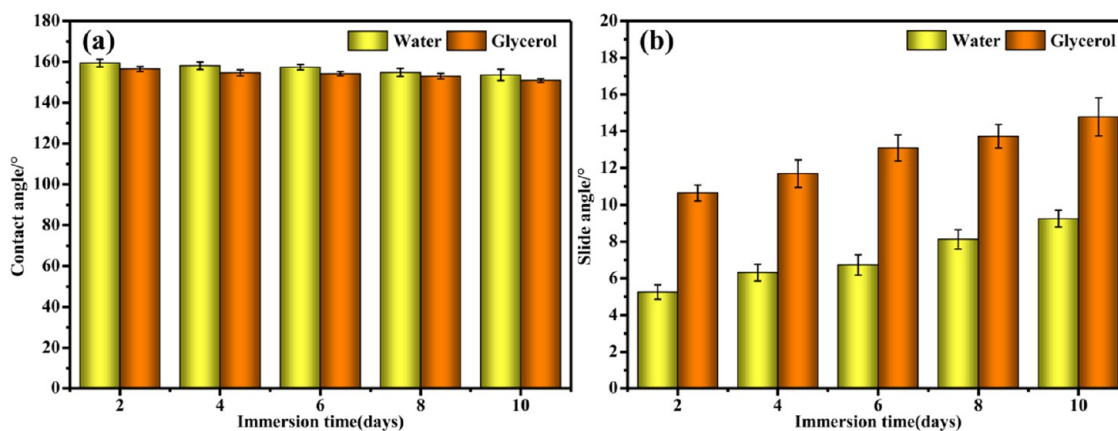
Figure 7. Glycerol immersion test. (a, b) CAs and SAs (glycerol, water) of the PTFE/SiO$_2$@CTMS&Na$_2$SiO$_3$-ATP composite coating soaked in glycerol for different times.
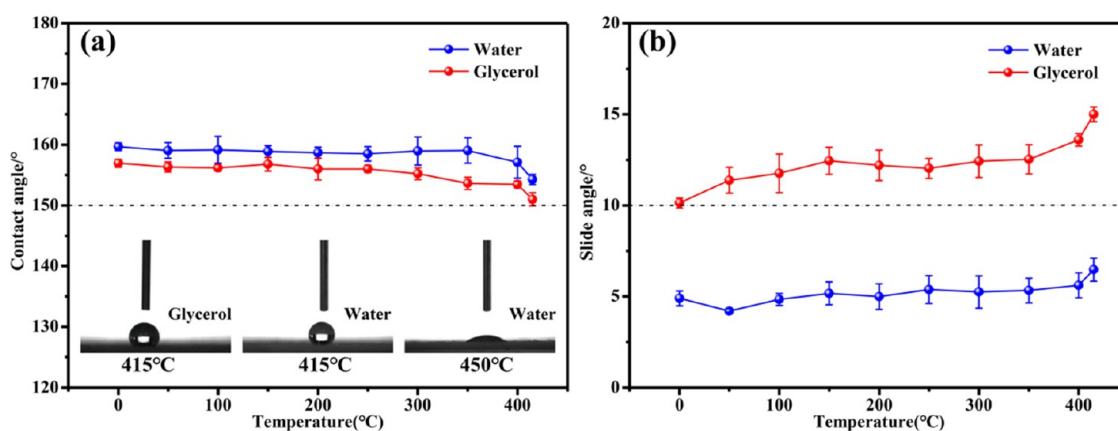
Figure 8. High-temperature resistance test. (a, b) CAs and SAs (water, glycerol) of the PTFE/SiO$_2$@CTMS&Na$_2$SiO$_3$-ATP composite coating after treatment at different temperatures.

3.5. Analysis of High-Temperature Resistance. The surface wettability after holding the composite coating at different temperatures for 2 h is shown in Figure 8. The PTFE/SiO$_2$@CTMS&Na$_2$SiO$_3$-ATP composite coating had excellent moisture resistance at 415 °C and maintained high CAs (water, glycerol). But the SAs of glycerol were increased from 10 ± 0.3 to 15 ± 0.4°. When the temperature reached 450 °C, the coating became powdered and lost superamphiphobic properties. The coating had moisture resistance in a wide temperature range on account of sodium silicate and modified ATP.[51−54]

3.6. Analysis of Heat Transfer Performance. In some application scenarios, superamphiphobic coatings require excellent thermal insulation, such as the shell wall of the heat exchanger. With the increase of the modified nanosilica filler, the thermal conductivity of the coating gradually decreased from 0.02 to 0.012 W/(m·k) (Figure 9a). Figure 9b shows the random particle distribution of the composite coating with 47.87 wt % modified nanosilica. Due to the increase of the content of modified nanosilica with low thermal conductivity, the path of thermal conductivity is formed in the coating to delay the heat conduction, which is beneficial for low thermal conductivity of the coating.[55] It proved the existence of the heat conduction path by finite element analysis. The physical parameters of the model material are shown in Table S2. By the heat flux distribution, it is clearly observed that with the increase of the content of low thermal conductive particles, it is easier to form a connected heat flux

path inside the model (Figure 10d−f). In addition, the heat flux value of the modified nanosilica filler is lower than those of other parts. As shown in Figure 10a−c, when the content of low thermal conductive particles increases from 0 to 47.87%, it slows down the heat transfer rates and increases the temperature difference to 1.2 °C on two sides of the model. This slowing down of the heat transfer process is observed by infrared thermography (Figure 9c), and the filler with low thermal conductivity has a certain effect on reducing the thermal conductivity of the coating. Accordingly, the results indicate that the PTFE/SiO$_2$@CTMS&Na$_2$SiO$_3$-ATP composite coating is suitable for heat insulation.

3.7. Analysis of Mechanical Performance. The mechanical performance of the PTFE/SiO$_2$@CTMS&Na$_2$SiO$_3$-ATP composite coating contains wear resistance, adhesion, and impact resistance. The wear resistance of the prepared composite coating was evaluated by the sandpaper abrasion test. The rough surface of sandpaper (800 mesh) contacted the coating surface, and the sandpaper was pulled back and forth, which was recorded as one time (Figure 11). After 10 cycles of the test, the PTFE/SiO$_2$@CTMS composite coating lost superamphiphobicity for glycerol (CAs = 149 ± 1°, SAs = 19 ± 0.5°) and water (CAs = 152 ± 1.5°, SAs = 11 ± 0.6°). Furthermore, after 20 cycles, the SAs of the PTFE/SiO$_2$@CTMS composite coating increased rapidly from 6 ± 0.8 to 16 ± 1° for water and from 11 ± 0.6 to 24 ± 1.8° for glycerol (Figure 12a,b). The
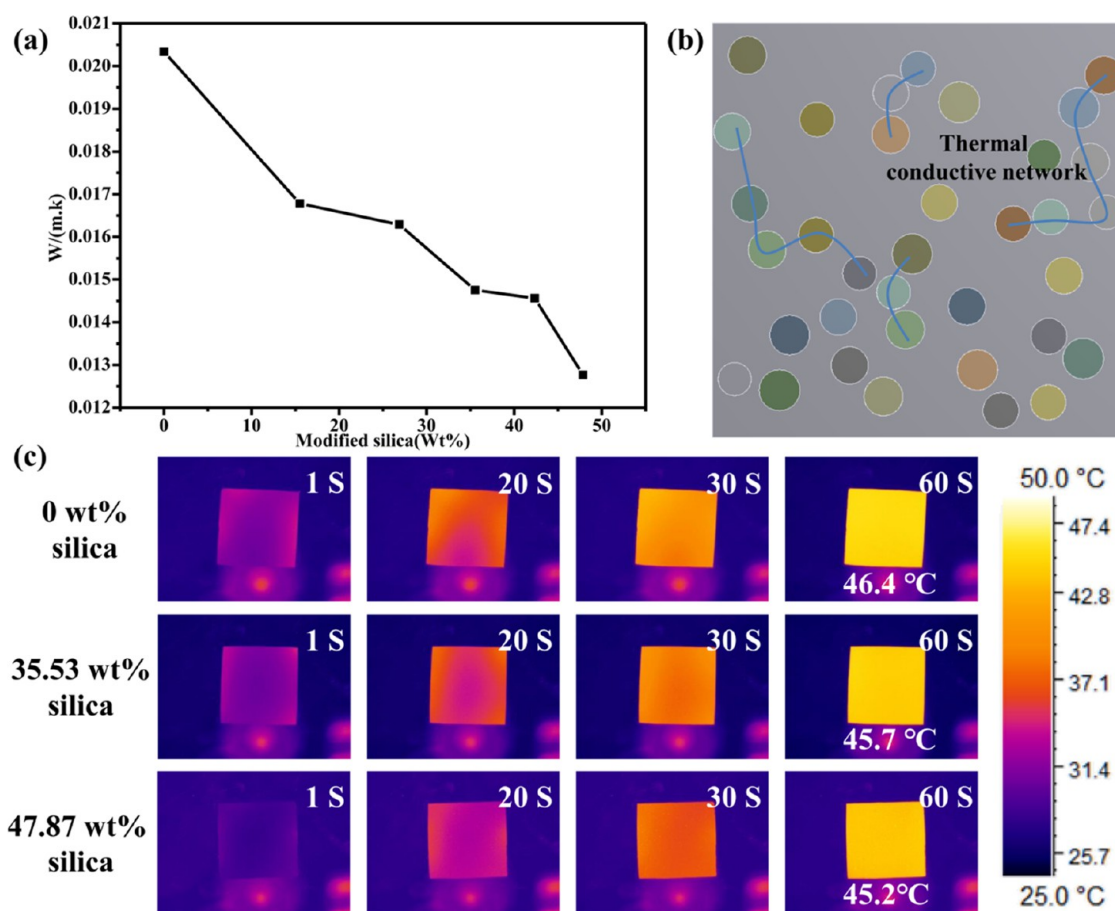
Figure 9. Thermal conductivity and temperature distribution. (a) Thermal conductivity of the coatings with different contents of modified silica nanoparticles. (b) Heat conduction mechanism of the PTFE/SiO$_2$@CTMS&Na$_2$SiO$_3$-ATP composite coating. (c) Infrared thermography.
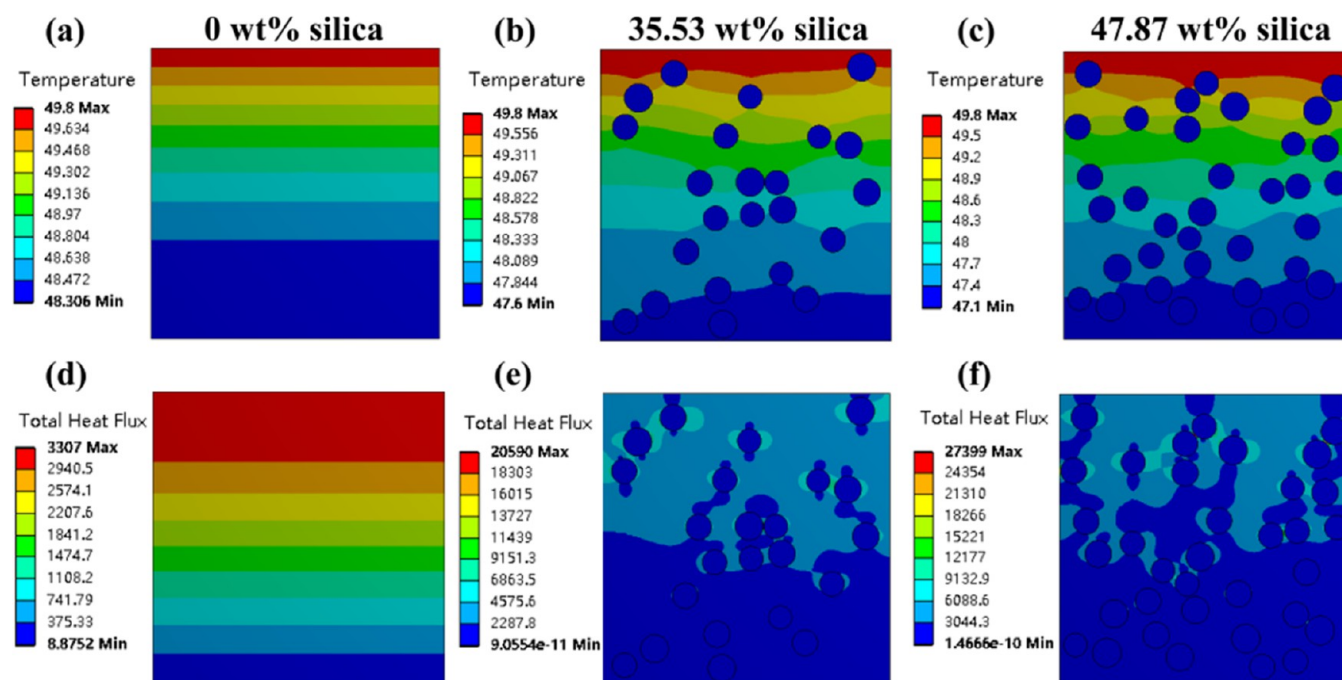
Figure 10. Finite element analysis. (a–c) The temperature distribution. (d–f) The heat flux distribution.

hardness of the PTFE/SiO$_2$@CTMS composite coating is regarded as 2B (Figures S9 and S10a,b). Even though the PTFE/SiO$_2$@CTMS composite coating possessed the wear-

resistant lubrication effect of nanosilica, it was unable to match the suitable hardness of the coating to cannot resist the cyclic damage of the rough surface of sandpaper many times.
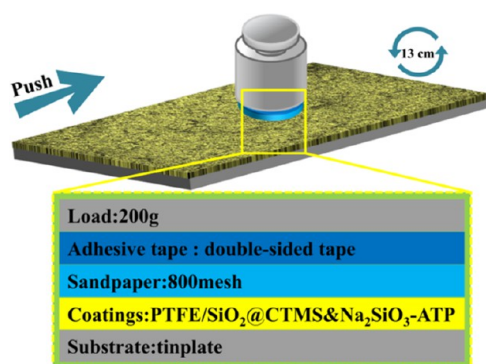
Figure 11. Process of the coating wear resistance test.

However, compared with the PTFE/SiO$_2$@CTMS composite coating, the PTFE/SiO$_2$@CTMS&Na$_2$SiO$_3$-ATP composite coating still had high repellency to water (CAs = 152 ± 0.8°, SAs = 11 ± 0.9°) and glycerol (CAs = 149 ± 0.7°, SAs = 22 ± 0.6°) after 140 cycles (Figure 12c,d). The wear resistance of the PTFE/SiO$_2$@CTMS&Na$_2$SiO$_3$-ATP composite coating is about 14 times that of the PTFE/SiO$_2$@CTMS composite coating. The excellent mechanical robustness of the composite coating was due to the introduction of sodium silicate and modified ATP, which made the hardness of the PTFE/SiO$_2$@CTMS&Na$_2$SiO$_3$-ATP composite coating reach 6H (Figure S10c,d). Meanwhile, the modified nanosilica of wear-resistant lubrication was tightly embedded in the film surface (Figure 5b), and it was not easy to be taken away by the rough surface of sandpaper when sliding.[56,57] High hardness and lubrication promote the PTFE/SiO$_2$@CTMS&Na$_2$SiO$_3$-ATP composite

coating to show excellent wear resistance and durable moisture resistance. As shown in Figure 13c,d, the composite coating surface was not damaged in a large area, and some emulsion protrusions were slightly worn. According to the comparison of the 3D surface morphology between the composite coating and the worn composite coating (after the wear resistance test of 140 cycles; Figure 13a,b), the arithmetic mean deviation of the profile (Ra) had little difference. It was basically consistent with the SEM of the composite coating before and after abrasion. The results indicated that the coating had excellent wear resistance.

The practical application of superamphiphobic coatings is inseparable from excellent adhesion and impact resistance. The coating adhesion is used to evaluate the adhesion index between the film and the substrate. Furthermore, the impact resistance is regarded as the ability to resist external deformation and cracking, which reflects the adhesion of the coating for the side. According to the paints and varnishes—cross-cut test (Figure 14f), to evaluate film adhesion, the surface of the PTFE/SiO$_2$@CTMS&Na$_2$SiO$_3$-ATP composite coating was marked as a 2 mm × 2 mm small square by a wallpaper knife to press the surface of the composite coating with 3M test grade tape for 3 min and then tore it quickly (repeated three times). It was clearly observed that the surface of the composite coating was not damaged before and after the adhesion of 3M test grade tape, which was classified as grade 1 adhesion (Figure 14a,b). The firm adhesion of the composite coating is mainly attributed to the interlocking effect of the network structure of PTFE, modified silica, sodium silicate, and modified ATP. Moreover, the PTFE/SiO$_2$@CTMS&Na$_2$SiO$_3$-ATP composite coating still had super-
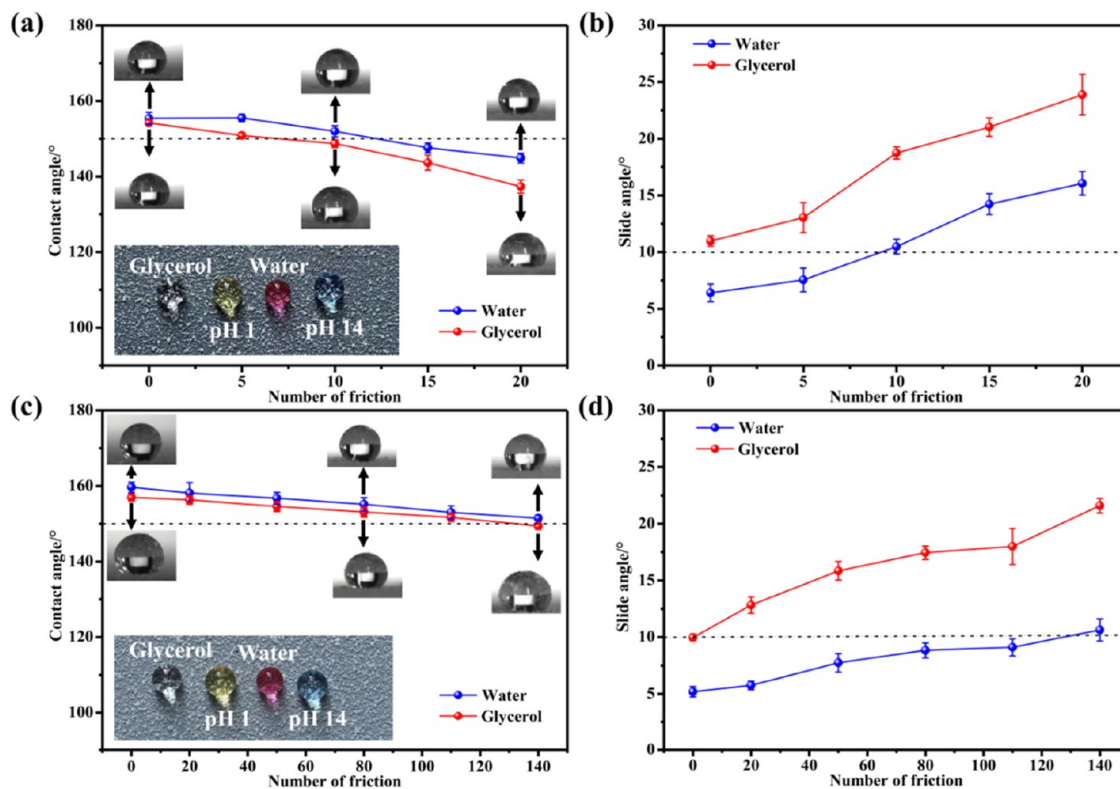
Figure 12. Abrasion resistance test. (a, b) CAs and SAs (glycerol, water) of the PTFE/SiO$_2$@CTMS composite coating after different cycle wear times. (c, d) CAs and SAs (glycerol, water) of the PTFE/SiO$_2$@CTMS&Na$_2$SiO$_3$-ATP composite coating after different cycle wear times. Inset: optical images of water, pH 1, pH 14, and glycerol droplets on the coating after abrasion.
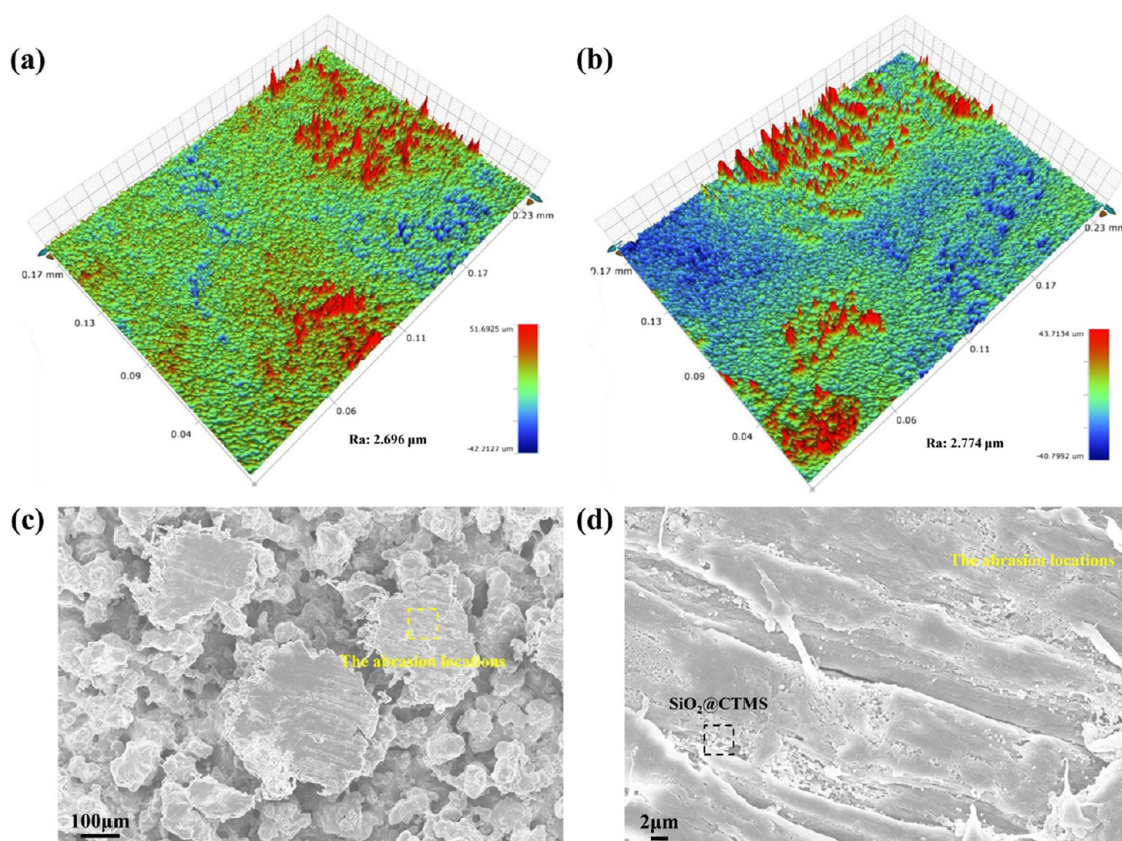
Figure 13. Morphological analysis of the PTFE/SiO$_2$@CTMS&Na$_2$SiO$_3$-ATP composite coating. (a) 3D surface morphology images of the composite coating. (b) 3D surface morphology images of the composite coating after the wear resistance test. (c, d) SEM of the composite coating and the emulsion protrusion after the wear resistance test.
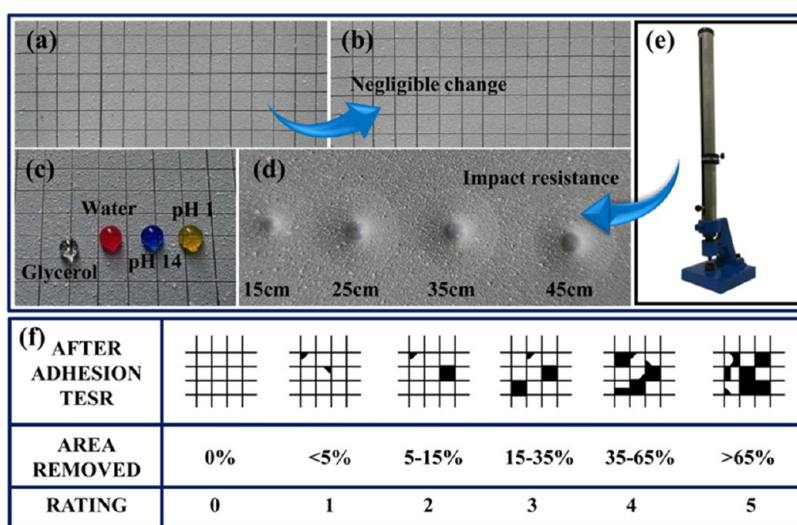
Figure 14. Test of the mechanical properties of the PTFE/SiO$_2$@CTMS&Na$_2$SiO$_3$-ATP composite coating. (a, b) PTFE/SiO$_2$@CTMS&Na$_2$SiO$_3$-ATP composite coating before and after the cross-cut tape test. (c) Optical images of water, pH 1, pH 14, and glycerol droplets on the coating after the cross-cut tape test. (d, e) The composite coating was impacted by a heavy hammer with different heights. (f) GB/T 9286.

amphiphobicity after the cross-cut test (Figure 14c). Marks were left on the surface of PTFE/SiO$_2$@CTMS&Na$_2$SiO$_3$-ATP composite coating at different heights (Figure 14d,e). With the increase of height (15−45 cm), deeper marks were left on the coating surface, but the surface of the composite coating was not cracked. It is indicated that the PTFE/SiO$_2$@

CTMS&Na$_2$SiO$_3$-ATP composite coating has excellent cracking resistance and adhesion.

3.8. Analysis of Corrosion Resistance. For the sake of exploring the corrosion resistance of the superamphiphobic coatings from a macroeconomic perspective, acid−base immersion experiments were conducted. The PTFE/SiO$_2$@ CTMS&Na$_2$SiO$_3$-ATP composite coating was soaked in
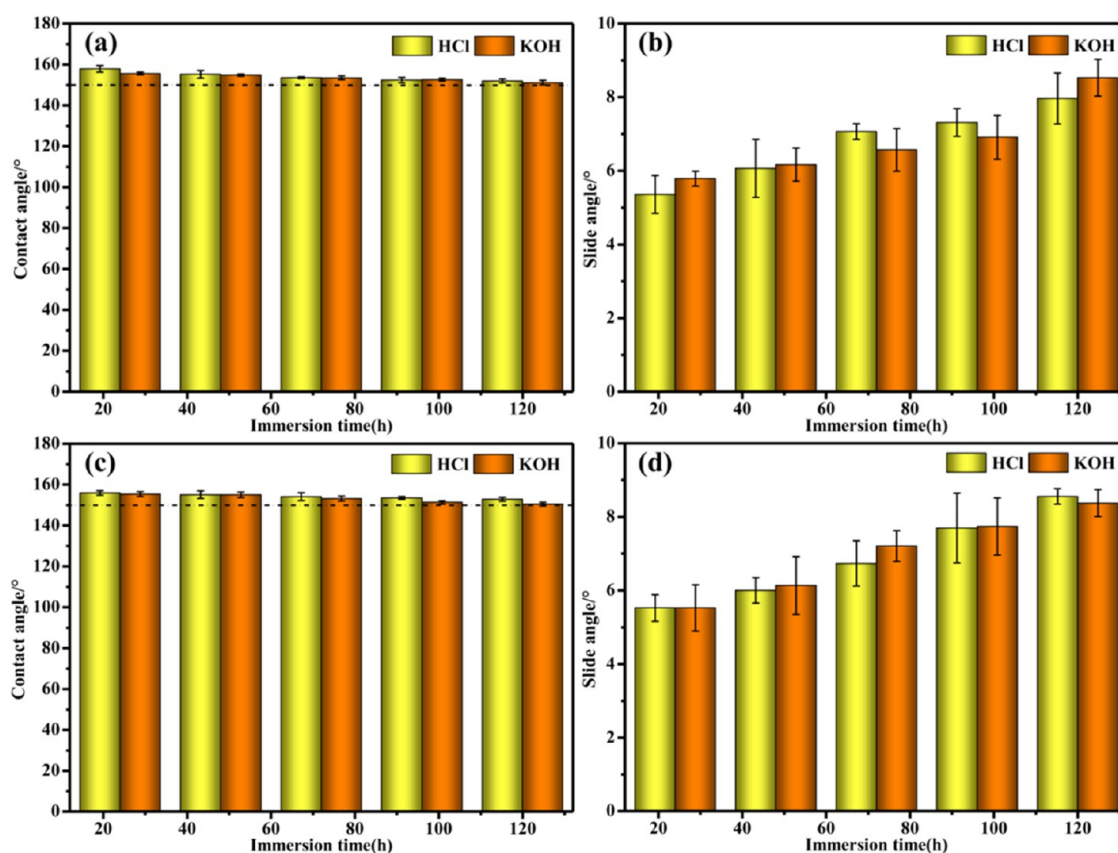
Figure 15. Acid−base immersion test. (a, b) CAs and SAs (pH 1, pH 14) of the PTFE/SiO$_2$@CTMS&Na$_2$SiO$_3$-ATP composite coating soaked in a pH 1 solution for different times. (c, d) CAs and SAs (pH 1, pH 14) of the PTFE/SiO$_2$@CTMS&Na$_2$SiO$_3$-ATP composite coating soaked in a pH 14 solution for different times.

solutions of hydrochloric acid (pH 1) and potassium hydroxide (pH 14) for different times (24, 48, 72, 96, and 120 h). The wettability of the PTFE/SiO$_2$@CTMS&Na$_2$SiO$_3$-ATP composite coating was measured for hydrochloric acid (pH 1) and potassium hydroxide (pH 14) so as to evaluate the repellency of corrosive droplets. It displayed that the composite coating was soaked in hydrochloric acid (pH 1) after 120 h immersion, and the CAs of the PTFE/SiO$_2$@CTMS&Na$_2$SiO$_3$-ATP composite coating were still greater than 150°, which were reduced from 158 ± 1.6 to 152 ± 1° for hydrochloric acid and from 156 ± 0.9 to 151 ± 1° for potassium hydroxide. The SAs were less than 10°, which were increased for hydrochloric acid (5 ± 0.5 to 8 ± 0.7°) and potassium hydroxide (6 ± 0.2 to 9 ± 0.5°, Figure 15a,b). The changing trend of the test results soaked in potassium hydroxide (pH 14) was basically the same as that soaked in hydrochloric acid (pH 1) after 120 h (Figure 15c,d). The long-term macroscopic excellent liquid repellency was closely related to the microscopic morphology. By observing the morphology of the coating after immersing in hydrochloric acid and potassium hydroxide for 120 h, it was found that the overall morphology of the coating was not damaged, and it was consistent with the morphology before immersion (Figure 16). It was indicated that hydrochloric acid (pH 1) and potassium hydroxide (pH 14) did not damage the PTFE/SiO$_2$@CTMS&Na$_2$SiO$_3$-ATP composite coating with excellent corrosion resistance within 120 h. Therefore, the PTFE/SiO$_2$@CTMS&Na$_2$SiO$_3$-ATP composite coating has excellent chemical stability in harsh corrosive environments.

To further analyze the corrosion resistance of the PTFE/SiO$_2$@CTMS&Na$_2$SiO$_3$-ATP composite coating, the corrosion prevention efficiency of the composite coating in sodium chloride solution (3.5 wt %) was studied. The typical potentiodynamic polarization curve was obtained (Figure 17a). The electrochemical parameters were obtained from the polarization curve (Table S3). Electrochemical parameters include corrosion potential (E_{corr}), corrosion current density (I_{corr}), corrosion rate (C.R.), and protection efficiency (P.E.). Compared with pure tinplate, the corrosion current densities of PTFE/SiO$_2$@CTMSand PTFE/SiO$_2$@CTMS&Na$_2$SiO$_3$-ATP composite coatings were reduced to 1.256×10^{-5} and 1.012×10^{-5} A/cm^2, respectively. Moreover, the corrosion potential of the PTFE/SiO$_2$@CTMS&Na$_2$SiO$_3$-ATP composite coating has achieved a significant positive shift to −0.23 V. The Nyquist spectra of the PTFE/SiO$_2$@CTMS&Na$_2$SiO$_3$-ATP composite coating have a large semicircle diameter, corresponding to a lower corrosion rate (Figure 17b). Therefore, corrosion resistance is the best. The electrochemical impedance spectra results are consistent with the polarization curve results, both of which show that the corrosion resistance of the PTFE/SiO$_2$@CTMS&Na$_2$SiO$_3$-ATP composite coating is superior to that of the PTFE/SiO$_2$@CTMS composite coating. The prepared superamphiphobic coatings had corrosion resistance, which was related to the internal structure of the coating and the formation of cavitation on the surface. The surface of the PTFE/SiO$_2$@CTMS&Na$_2$SiO$_3$-ATP composite coating had many protrusions with micro/nanostructures similar to the lotus leaf surface. These
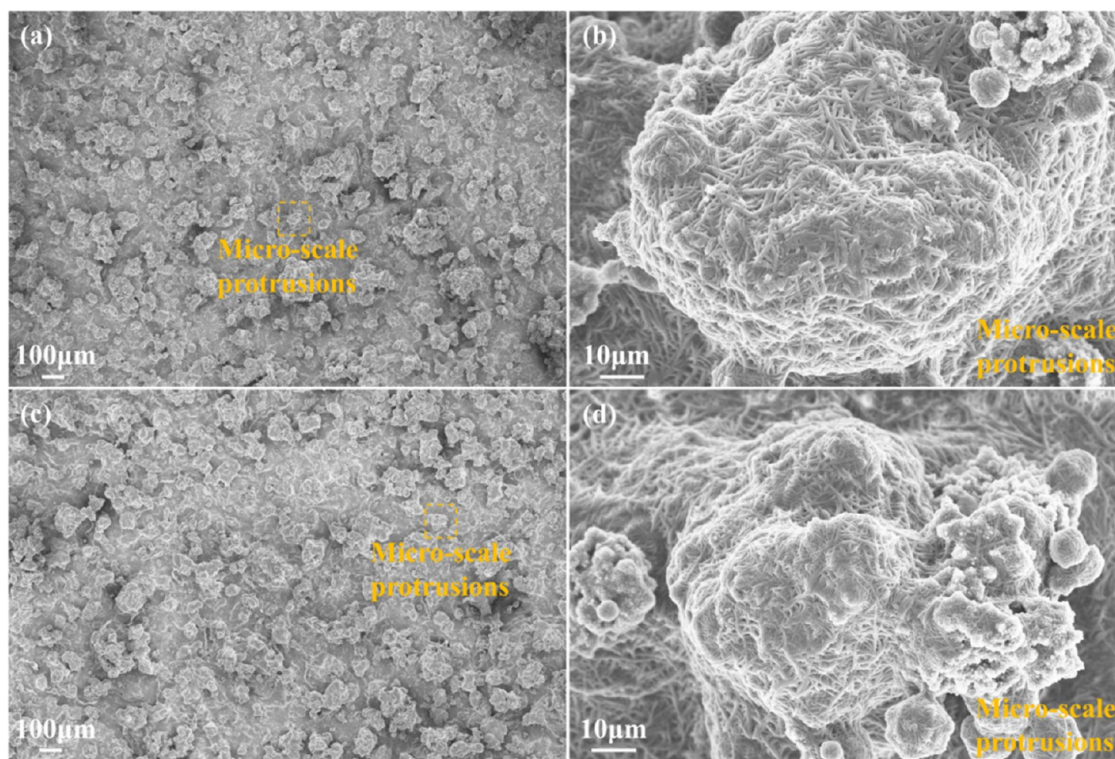
Figure 16. SEM of the PTFE/SiO$_2$@CTMS&Na$_2$SiO$_3$-ATP composite coating after the acid−base immersion test. (a, b) SEM of the PTFE/SiO$_2$@CTMS&Na$_2$SiO$_3$-ATP composite coating after soaking in a pH 1 solution for 120 h. (c, d) SEM of the PTFE/SiO$_2$@CTMS&Na$_2$SiO$_3$-ATP composite coating after soaking in a pH 14 solution for 120 h.
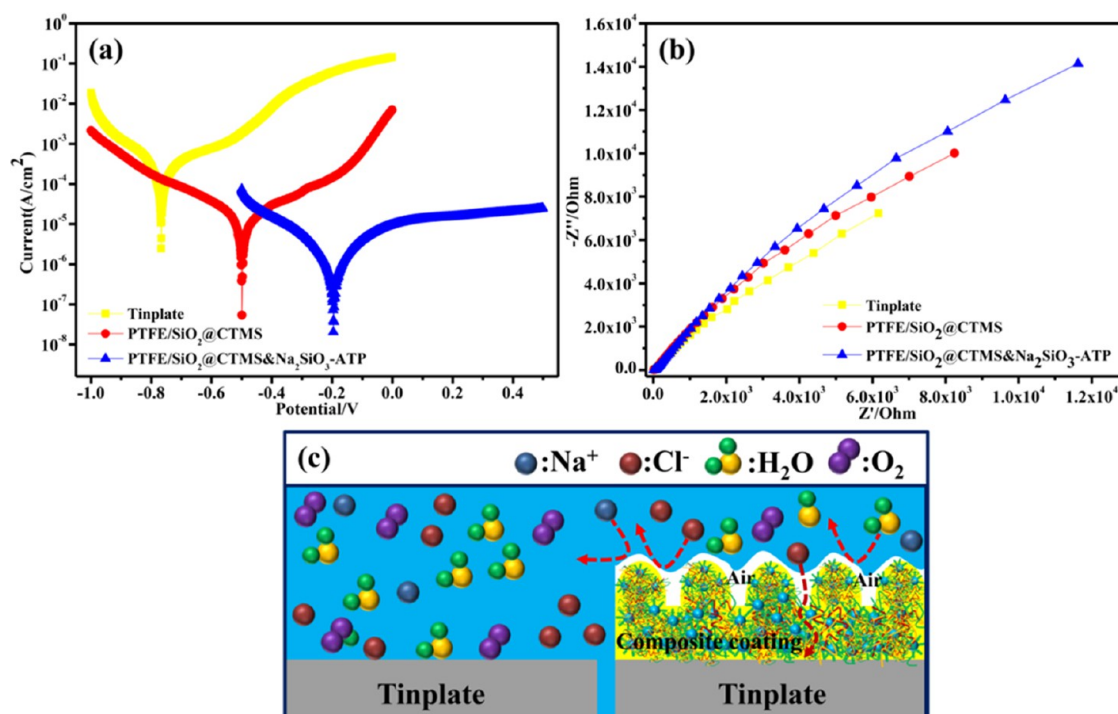
Figure 17. Corrosion resistance test. (a) Potentiodynamic polarization curves. (b) Nyquist plots (c) Anticorrosion principle.

protrusions with micro/nanostructures intercepted air and formed stable cavitation, which prevented the composite coating surface from being wet and prevented corrosive substances from corroding the substrate (Figure 17c). The modified silica as a physical barrier inside the coating prolonged the time for corrosive substances to pass through the coating and reach the substrate. The physical barrier and stable cavitation make the film have excellent corrosion resistance. Hence, the ability of a composite coating to stand

up to the severe corrosive environment is conducive to its application in a practical factory environment..

4. CONCLUSIONS

In summary, the waterborne dispersion was successfully prepared by simple mechanical dispersion of emulsions (PTFE emulsion, dispersion of modified silica, sodium silicate, and modified ATP). The four kinds of emulsions that were mixed together can effectively solve the dispersity of waterborne superamphiphobic coatings. The dispersion was sprayed and cured at 310 °C for 15 min to obtain a surface with superior repellency to water (CAs = 160 ± 0.7°, SAs = 4 ± 0.2°) and glycerol (CAs = 156 ± 0.9°, SAs = 10 ± 0.7°). The PTFE/SiO$_2$@CTMS&Na$_2$SiO$_3$-ATP composite coating showed strong adhesive ability (grade 1 according to the GB/T9286), high hardness (6H), superior antifouling performance, excellent impact resistance, high-temperature resistance (<415 °C), and heat insulation. Remarkably, under a load of 200 g, the composite coating still had remarkable repellency to water (CAs = 152 ± 0.8°, SAs = 11 ± 0.9°) and glycerol (CAs = 149 ± 0.7°, SAs = 22 ± 0.6°) after 140 cycles of wear. Furthermore, the PTFE/SiO$_2$@CTMS&Na$_2$SiO$_3$-ATP composite coating was separately soaked in hydrochloric acid (pH 1) and potassium hydroxide (pH 14) for 120 h, and it still showed excellent repellency to hydrochloric acid (pH 1) and potassium hydroxide (pH 14). With multifaceted robustness and scalability, the PTFE/SiO$_2$@CTMS&Na$_2$SiO$_3$-ATP composite coating possesses potential usage in impact resistance, heat insulation, high-temperature service, and chemical corrosion.

■ ASSOCIATED CONTENT

Ⓢ Supporting Information

The Supporting Information is available free of charge at https://pubs.acs.org/doi/10.1021/acsomega.2c06145.

Slurry dumping test (Movie S1) (MP4)

Coating was repeatedly immersed in glycerol 100 times (Movie S2) (MP4)

Glycerol dumping test (Movie S2) (MP4)

Dispersion of modified silica nanoparticles (Figure S1); dispersion of the PTFE/SiO2@CTMS&ATP composite coating (Figure S2); influence of 192 and 360 nm modified silica on the wettability of composite coatings (Figure S3); surface of the PTFE/SiO$_2$@CTMS&Na$_2$SiO$_3$-ATP composite coating with 52.43 wt % modified silica (Figure S4); thickness of the composite coating (Figure S5); FT-IR spectra and XRD spectra of the PTFE/SiO$_2$@CTMS&Na$_2$SiO$_3$-ATP composite coating (Figure S6); standard card of substance to modified ATP and PTFE (Figure S7); standard card of substance to the PTFE/SiO$_2$@CTMS&Na$_2$SiO$_3$-ATP composite coating (Figure S8); Functional group details of FT-IR spectra (Table S1); Physical parameters of the model material (Table S2); pencil hardness tester (Figure S9); SEM of the composite coating after crossing by a pencil hardness tester (Figure S10); and potentiodynamic polarization parameter values for uncoated and coated tinplate substrates (Table S3) (PDF)

■ AUTHOR INFORMATION

Corresponding Author

Guoyu Ren − *School of Chemistry and Chemical Engineering, Yulin University, Yulin, Shaanxi 719000, P. R. China; Shaanxi Key Laboratory of Low Metamorpcoal Clean Utilizationhic, Yulin University, Yulin, Shaanxi 719000, P. R. China;* ⓞ orcid.org/0000-0002-7683-7048; Email: rgy5617@163.com

Authors

Zeting Qiao − *School of Chemistry and Chemical Engineering, Yulin University, Yulin, Shaanxi 719000, P. R. China*

Xiaodong Chen − *School of Chemistry and Chemical Engineering, Yulin University, Yulin, Shaanxi 719000, P. R. China*

Yanli Gao − *School of Chemistry and Chemical Engineering, Yulin University, Yulin, Shaanxi 719000, P. R. China;* ⓞ orcid.org/0000-0001-7830-6016

Yun Tuo − *School of Chemistry and Chemical Engineering, Yulin University, Yulin, Shaanxi 719000, P. R. China*

Cuiying Lu − *School of Chemistry and Chemical Engineering, Yulin University, Yulin, Shaanxi 719000, P. R. China; Shaanxi Key Laboratory of Low Metamorpcoal Clean Utilizationhic, Yulin University, Yulin, Shaanxi 719000, P. R. China*

Complete contact information is available at:
https://pubs.acs.org/10.1021/acsomega.2c06145

Author Contributions

Z.Q.: methodology, data curation, formal analysis, writing—original draft, and validation. G.R.: investigation, writing—review & editing. X.C.: investigation and writing—review & editing. Y.G.: conceptualization and resources. Y.T.: methodology and investigation. C.L.: methodology and writing—review & editing.

Notes

The authors declare no competing financial interest.

■ REFERENCES

(1) Sun, S.; Li, H.; Guo, Y.; Mi, H.; He, P.; Zheng, G.; Liu, C.; Shen, C. Superefficient and robust polymer coating for bionic manufacturing of superwetting surfaces with "rose petal effect" and "lotus leaf effect". *Prog. Org. Coat.* **2021**, *151*, No. 106090.

(2) Wang, P.; Zhao, T.; Bian, R.; Wang, G.; Liu, H. Robust Superhydrophobic Carbon Nanotube Film with Lotus Leaf Mimetic Multiscale Hierarchical Structures. *ACS Nano* **2017**, *11*, 12385−12391.

(3) Wang, S.; Wang, Y.; Zou, Y.; Chen, G.; Ouyang, J.; Jia, D.; Zhou, Y. Scalable-Manufactured Superhydrophobic Multilayer Nanocomposite Coating with Mechanochemical Robustness and High-Temperature Endurance. *ACS Appl. Mater. Interfaces* **2020**, *12*, 35502−35512.

(4) Zhang, M.; Feng, S.; Wang, L.; Zheng, Y. Lotus effect in wetting and self-cleaning. *Biotribology* **2016**, *5*, 31−43.

(5) Chen, B.; Lv, Z.; Guo, F.; Huang, Y. Integrated CNTs/SiO$_2$ nano-additives on SBS polymeric superhydrophobic coatings for self-cleaning. *Surf. Eng.* **2019**, *36*, 601−606.

(6) Miao, S.; Xiong, Z.; Zhang, J.; Wu, Y.; Gong, X. Polydopamine/SiO$_2$ Hybrid Structured Superamphiphobic Fabrics with Good Photothermal Behavior. *Langmuir* **2022**, *38*, 9431−9440.

(7) Li, W.; Liang, Z.; Dong, B.; Tang, H. Transmittance and self-cleaning polymethylsiloxane coating with superhydrophobic surfaces. *Surf. Eng.* **2020**, *36*, 574−582.

(8) Xiong, Z.; Yu, H.; Gong, X. Designing Photothermal Superhydrophobic PET Fabrics via In Situ Polymerization and 1,4-Conjugation Addition Reaction. *Langmuir* **2022**, *38*, 8708−8718.

(9) Wu, B.; Ye, L.; Zhang, Z.; Zhao, X. Facile construction of robust super-hydrophobic coating for urea-formaldehyde foam: Durable hydrophobicity and Self-cleaning ability−ScienceDirect. *Composites, Part A* **2020**, *132*, No. 105831.

(10) Aljallis, E.; Sarshar, M. A.; Datla, R.; Sikka, V.; Jones, A.; Choi, C. H. Experimental study of skin friction drag reduction on superhydrophobic flat plates in high Reynolds number boundary layer flow. *Phys. Fluids* **2013**, *25*, No. 025103.

(11) Lauga, E.; Stone, H. A. Effective slip in pressure-driven Stokes flow. *J. Fluid Mech.* **2003**, *489*, 55−77.

(12) Kharitonov, A. P.; Simbirtseva, G. V.; Nazarov, V. G.; Stolyarov, V. P.; Dubois, M.; Peyroux, J. Enhanced anti-graffiti or adhesion properties of polymers using versatile combination of fluorination and polymer grafting. *Prog. Org. Coat.* **2015**, *88*, 127−136.

(13) Liu, H.; Zhu, Y.; Shang, Q. Q.; Xiao, G. M. Preparation of Water-Based Anti-Graffiti Polyurethane Coating. *Adv. Mater. Res.* **2013**, *634–638*, 2993−2996.

(14) Ye, X.; Hou, J.; Yan, X.; Wu, X. Development of a Transparent Coating to Enhance Self-Cleaning Capability and Strength in Conventional Paper. *J. Nanomater.* **2019**, *2019*, No. 3484239.

(15) Gao, X.; Guo, Z. Mechanical stability, corrosion resistance of superhydrophobic steel and repairable durability of its slippery surface. *J. Colloid Interface Sci.* **2018**, *512*, 239−248.

(16) Peng, C.-W.; Chang, K.-C.; Weng, C.-J.; Lai, M.-C.; Hsu, C.-H.; Hsu, S.-C.; Hsu, Y.-Y.; Hung, W. I.; Wei, Y.; Yeh, J.-M. Nano-casting technique to prepare polyaniline surface with biomimetic super-hydrophobic structures for anticorrosion application. *Electrochim. Acta* **2013**, *95*, 192−199.

(17) Qin, Y.; Li, Y.; Zhang, D.; Zhu, X. Stability and corrosion property of oil-infused hydrophobic silica nanoparticle coating. *Surf. Eng.* **2021**, *37*, 206−211.

(18) Yuan, R.; Wu, S.; Yu, P.; Wang, B.; Mu, L.; Zhang, X.; Zhu, Y.; Wang, B.; Wang, H.; Zhu, J. Superamphiphobic and Electroactive Nanocomposite toward Self-Cleaning, Antiwear, and Anticorrosion Coatings. *ACS Appl. Mater. Interfaces* **2016**, *8*, 12481−12493.

(19) Farhadi, S.; Farzaneh, M.; Kulinich, S. A. Anti-icing performance of superhydrophobic surfaces. *Appl. Surf. Sci.* **2011**, *257*, 6264−6269.

(20) Tourkine, P. M.; Merrer, L.; Quéré, D. Delayed Freezing on Water Repellent Materials. *Langmuir.* **2009**, *25*, 7214−7216.

(21) Wu, C.; Geng, H.; Tan, S.; Lv, J.; Wang, H.; He, Z.; Wang, J. Highly efficient solar anti-icing/deicing via a hierarchical structured surface. *Mater. Horiz.* **2020**, *7*, 2097−2104.

(22) Peng, J.; Yuan, S.; Geng, H.; Zhang, X.; Wang, H.; et al. Robust and multifunctional superamphiphobic coating toward effective anti-adhesion. *Chem. Eng. J.* **2022**, *428*, No. 131162.

(23) Chen, C.; Tian, Z.; Luo, X.; Jiang, G.; Hu, X.; Wang, L.; Peng, R.; Zhang, H.; Zhong, M. Cauliflower-like micro-nano structured superhydrophobic surfaces for durable anti-icing and photothermal de-icing. *Chem. Eng. J.* **2022**, *450*, No. 137936.

(24) Liu, Y.; Li, S.; Wang, Y.; Wang, H.; Gao, K.; Han, Z.; Ren, L. Superhydrophobic and superoleophobic surface by electrodeposition on magnesium alloy substrate: Wettability and corrosion inhibition. *J. Colloid Interface Sci.* **2016**, *478*, 164−171.

(25) Grozea, C. M.; Huang, S.; Liu, G. Water-based, heat-assisted preparation of water-repellent cotton fabrics using graft copolymers. *RSC Adv.* **2016**, *6*, 20135−20144.

(26) Zhang, J.; Gao, Z.; Li, L.; Li, B.; Sun, H. Waterborne Nonfluorinated Superhydrophobic Coatings with Exceptional Mechanical Durability Based on Natural Nanorods. *Adv. Mater. Interfaces* **2017**, *4*, No. 1700723.

(27) Liu, Z.-h.; Pang, X.; Wang, K.; Lv, X.; Cui, X. Super-hydrophobic Coatings Prepared by the in Situ Growth of Silicone Nanofilaments on Alkali-Activated Geopolymers Surface. *ACS Appl. Mater. Interfaces* **2019**, *11*, 22809−22816.

(28) Cunningham, M. F.; Campbell, J. D.; Fu, Z.; Bohling, J.; Leroux, J. G.; Mabee, W.; Robert, T. Future green chemistry and sustainability needs in polymeric coatings. *Green Chem.* **2019**, *21*, 4919−4926.

(29) Baidya, A.; Das, S. K.; Ras, R. H. A.; Pradeep, T. Fabrication of a Waterborne Durable Superhydrophobic Material Functioning in Air and under Oil. *Adv. Mater. Interfaces* **2018**, *5*, No. 1701523.

(30) Lozhechnikova, A.; Bellanger, H.; Michen, B.; Burgert, I.; Österberg, M. Surfactant-free carnauba wax dispersion and its use for layer-by-layer assembled protective surface coatings on wood. *Appl. Surf. Sci.* **2017**, *396*, 1273−1281.

(31) Aslanidou, D.; Karapanagiotis, I.; Panayiotou, C. Super-hydrophobic, superoleophobic coatings for the protection of silk textiles. *Prog. Org. Coat.* **2016**, *97*, 44−52.

(32) Chatzigrigoriou, A.; Manoudis, P. N.; Karapanagiotis, I. Fabrication of Water Repellent Coatings Using Waterborne Resins for the Protection of the Cultural Heritage. *Macromol. Symp.* **2013**, *331-332*, 158−165.

(33) Ioannis, K.; Diana, G.; Dimitra, A.; Aifantis, K. E. Facile method to prepare superhydrophobic and water repellent cellulosic paper. *J. Nanomater.* **2015**, *2015*, No. 219013.

(34) Liu, M.; Hou, Y.; Li, J.; Tie, L.; Guo, Z. An all-water-based system for robust superhydrophobic surfaces. *J. Colloid Interface Sci.* **2018**, *519*, 130−136.

(35) Li, Y.; Li, B.; Zhao, X.; Tian, N.; Zhang, J. Totally Waterborne, Nonfluorinated, Mechanically Robust, and Self-Healing Super-hydrophobic Coatings for Actual Anti-Icing. *ACS Appl. Mater. Interfaces* **2018**, *10*, 39391−39399.

(36) Zhao, X.; Hao, H.; Duan, Y.; Wang, J. A robust super-hydrophobic and highly oleophobic coating based on F-SiO$_2$-copolymer composites. *Prog. Org. Coat.* **2019**, *135*, 417−423.

(37) Lin, D.; Zhang, X.; Yuan, S.; Li, Y.; Xu, F.; Wang, X.; Li, C.; Wang, H. Robust Waterborne Superhydrophobic Coatings with Reinforced Composite Interfaces. *ACS Appl. Mater. Interfaces* **2020**, *12*, 48216−48224.

(38) Wang, J.; Cui, M.; Wang, D.; Liu, Y.; Cai, J.; Gu, Z.; Hu, C. Integration of superhydrophobicity and high durability in super-rough hard thin films. *Ceram. Int.* **2021**, *47*, 23653−23658.

(39) Ma, W.; Zhao, M.; Zhao, J.; Guo, Z.; Cui, Y.; Li, H. Preparation of superamphiphobic stainless steel surface by laser and perfluor-ooctanoic acid treatment. *Opt. Laser Technol.* **2022**, *154*, No. 108321.

(40) Garskaite, E.; Olov, K.; Zivile, S.; Aivaras, K.; Dennis, J.; Dick, S. Surface hardness and flammability of Na$_2$SiO$_3$ and nano-TiO$_2$ reinforced wood composites. *RSC Adv.* **2019**, *9*, 27973−27986.

(41) Kumar, S. P.; Takamori, S.; Araki, H.; Kuroda, S. Flame retardancy of clay-sodium silicate composite coatings on wood for construction purposes. *RSC Adv.* **2015**, *5*, 34109−34116.

(42) Balabanovich, A. I.; Schartel, B.; Knoll, U.; Artner, J.; Ciesielski, M.; Döring, M.; Perez, R.; Sandler, J.; Altstädt, V.; et al. Influence of the oxidation state of phosphorus on the decomposition and fire behaviour of flame-retarded epoxy resin composites. *Polymer* **2006**, *47*, 8495−8508.

(43) Morgan, A. B.; Gilman, J. W. An overview of flame retardancy of polymeric materials: application, technology, and future directions. *Fire Mater.* **2013**, *37*, 259−279.

(44) Mousavi, M. A.; Hassanajili, S.; Rahimpour, M. R. Synthesis of fluorinated nano-silica and its application in wettability alteration

near-wellbore region in gas condensate reservoirs. *Appl. Surf. Sci.* **2013**, *273*, 205−214.

(45) Zhu, J.; Liao, K. A Facile Method for Preparing a Superhydrophobic Block with Rapid Reparability. *Coatings* **2020**, *10*, 1202.

(46) Cassie, A. B. D.; Baxter, S. Wettability of porous surfaces. *Trans. Faraday Soc.* **1944**, *40*, 546−551.

(47) Yu, H.; Wu, M.; Duan, G.; Gong, X. One-step fabrication of eco-friendly superhydrophobic fabrics for high-efficiency oil/water separation and oil spill cleanup. *Nanoscale* **2022**, *14*, 1296−1309.

(48) Qu, M.; Ma, X.; He, J.; Feng, J.; Liu, S.; Yao, Y.; Hou, L.; Liu, X. Facile Selective and Diverse Fabrication of Superhydrophobic, Superoleophobic-Superhydrophilic and Superamphiphobic Materials from Kaolin. *ACS Appl. Mater. Interfaces.* **2017**, *9*, 1011−1020.

(49) Zhou, X.; Liu, J.; Liu, W.; Steffen, W.; Butt, H. J. Fabrication of Stretchable Superamphiphobic Surfaces with Deformation-Induced Rearrangeable Structures. *Adv. Mater.* **2022**, *34*, No. 2107901.

(50) Han, X.; Gong, X. In Situ, One-Pot Method to Prepare Robust Superamphiphobic Cotton Fabrics for High Buoyancy and Good Antifouling. *ACS Appl. Mater. Interfaces* **2021**, *13*, 31298−31309.

(51) Lee, S. J.; Thole, V. Investigation of modified water glass as adhesive for wood and particleboard: mechanical, thermal and flame retardant properties. *Eur. J. Wood Prod.* **2018**, *76*, 1427−1434.

(52) Pries, M.; Mai, C. Fire resistance of wood treated with a cationic silica sol. *Eur. J. Wood Prod.* **2013**, *71*, 237−244.

(53) Pawlowski, K. H.; Scharte, B. Flame retardancy mechanisms of triphenyl phosphate, resorcinol bis(diphenyl phosphate) and bisphenol A bis(diphenyl phosphate) in polycarbonate/acrylonitrile−butadiene−styrene blends. *Polym. Int.* **2007**, *56*, 1404−1414.

(54) Braun, U.; Horst, B.; Heinz, S.; Bernhard, S. Flame retardancy mechanisms of metal phosphinates and metal phosphinates in combination with melamine cyanurate in glass-fiber reinforced poly (1,4-butylene terephthalate): the influence of metal cation. *Polym. Adv. Technol.* **2008**, *19*, 680−692.

(55) Zhou, F.; Yang, L. An anisotropic thermal conductivity model for CNTs nanofluids by considering the discontinuity of nanotubes in thermal conduction path. *Int. Commun. Heat Mass Transfer.* **2021**, *128*, No. 105620.

(56) Jing, G. F.; Sheng, L. M.; Xin, H. Z.; Chang, Q. X.; Zhi, J. Y.; Dong, C.; Chun, S. M. Influence of solid lubricant WS_2 on the tribological properties of plasma electrolytic oxidation coating of ZL109. *Mater. Res. Express.* **2020**, *6*, No. 1265c8.

(57) Mirjavadi, S. S.; Alipour, M.; Emamian, S.; Kord, S.; Hamouda, A. M. S.; Koppad, P. G.; Keshavamurthy, R. Influence of TiO_2 nanoparticles incorporation to friction stir welded 5083 aluminum alloy on the microstructure, mechanical properties and wear resistance. *J. Alloys Compd.* **2017**, *712*, 795−803.